

## Characteristics of single metallic nanowire growth via a field-emission induced process

C. H. Oon

*Department of Electrical and Computer Engineering, National University of Singapore, 4 Engineering Drive 3, Singapore 117576, and Singapore-Massachusetts Institute of Technology (MIT) Alliance, 4 Engineering Drive 3, Singapore 117576*

S. H. Khong

*Physics Department, National University of Singapore, 2 Science Drive 3, Singapore 117542*

C. B. Boothroyd

*Institute of Materials Research & Engineering, 3 Research Link, Singapore 117602*

J. T. L. Thong<sup>a)</sup>

*Department of Electrical and Computer Engineering, National University of Singapore, 4 Engineering Drive 3, Singapore 117576*

(Received 4 August 2005; accepted 31 January 2006; published online 27 March 2006)

The growth and characteristics of metallic nanowires formed by field emission in the presence of organometallic precursors are studied. At low growth currents, single nanowires can be formed, which allows a systematic study of the growth characteristics, and wire morphology, structure, and composition. The major role of metal ion deposition in forming the metallic core is demonstrated experimentally, while the formation of the carbonaceous overcoat results from the deposition of neutral atoms from the precursor dissociation process. Transmission electron microscope analysis of tungsten nanowires shows that the core is polycrystalline, with columnar grains dominating the microstructure for thin wires, while larger diameter nanowires are straddled by multiple grains with a wider range of sizes. The axial and radial growth rates of tungsten nanowires as a function of growth current were studied and can be accounted for by assuming a situation in which the rate of ion formation just ahead of the growing tip is supply-rate limited. At higher growth currents, forking and branching phenomena were found to be increasingly probable, and hence, a key to the growth of single, well-defined nanowires is to keep the growth current low. Thermal decomposition of the precursor can also contribute to nanowire growth, and evidence for this mechanism was found in the cases of precursors where autocatalytic decomposition is known to result in metal deposition at relatively low temperatures. © 2006 American Institute of Physics. [DOI: 10.1063/1.2181281]

### I. INTRODUCTION

Nanowires have been the subject of intense research activity in recent years,<sup>1</sup> with burgeoning interest that has grown with the discovery of the carbon nanotube,<sup>2</sup> and later developments in semiconductor<sup>3</sup> and metal oxide nanowires.<sup>1</sup> Techniques to fabricate metallic nanowires have also been developed, many of which involve electrochemical deposition on such templates as porous membranes,<sup>4–6</sup> organic nanotube templates,<sup>7</sup> surface step edges,<sup>8</sup> and biotemplates.<sup>9</sup> While many examples of bulk nanowire synthesis have been reported, subsequent application of nanowires to electrical devices or circuits often require the harvesting, redeposition, and alignment of the nanowires to electrodes. Methods to align nanowires include the use of fluid alignment,<sup>10</sup> and dielectrophoretic alignment.<sup>11</sup> In an alternative approach, the role of an electric field to align carbon nanotubes during growth has been well established in forming vertically aligned<sup>12</sup> and laterally directed tubes.<sup>13</sup> More recently, metallic nanowires have been demonstrated to grow between biased electrodes in an aqueous solution.<sup>14</sup>

We have previously demonstrated the ability to grow single metallic nanowires through a field-emission induced process in the presence of an organometallic precursor.<sup>15</sup> These nanowires consist of a metallic core coated with a carbonaceous layer that is insulating and which additionally protects the core from oxidation.<sup>15</sup> We had previously demonstrated the use of these nanowires as nanotips for scanning probe microscopy,<sup>16–18</sup> and nanointerconnects.<sup>19</sup> Other potential uses could be for field emitters and exploitation of their mechanical properties. The technique stems from early observations of carbon and subsequently tungsten needlelike growth resulting from a glow discharge in the ambience of an organic or organometallic gas.<sup>20,21</sup> Okuyama and his co-workers subsequently studied the growth and microstructure of tungsten, molybdenum, and chromium “needles” from their respective carbonyls at room and high temperatures.<sup>22–27</sup> From transmission electron microscope (TEM) electron diffraction studies, the massive dendritic growth initiated on unheated cathodes is found to comprise an agglomeration of unoriented metal crystallites. With heated cathodes, single-crystal whiskers of larger diameter were found to form. While attempts have been made to un-

<sup>a)</sup>Author to whom correspondence should be addressed; electronic mail: elettl@nus.edu.sg

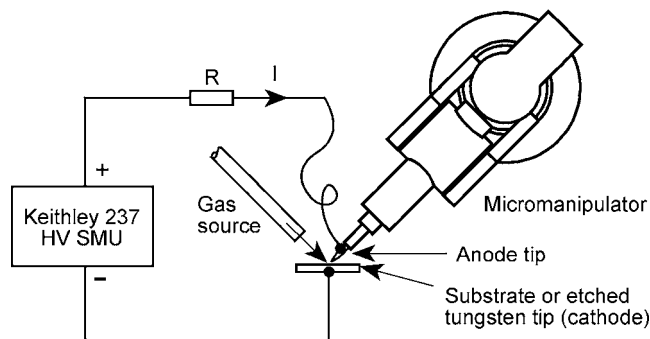


FIG. 1. Experimental setup. The etched anode tip is biased at a positive bias by a high-voltage source-measurement unit (SMU). Series resistor  $R$  is positioned near the tip and limits the current flow to prevent fast transients from destroying the nanowire.

derstand the underlying mechanisms of growth process,<sup>26,28</sup> a systematic study has been hindered by the uncontrolled growth of a mass of needles.

In Okuyama's experiments, needles were obtained from a field-emission cathode, operating either in the cold field-emission or thermal field-emission mode. The metal carbonyl vapor pressure is typically in the order of  $10^{-2}$ – $10^{-1}$  mbar, with total emission currents of up to 1 mA. Earlier work by Linden *et al.*<sup>21</sup> had reported emission currents of around several milliamps. A corona discharge was observed as light emission around the cathode point.<sup>25,26</sup> A different type of growth was reported for operation in the arc-discharge regime.<sup>26</sup> It was proposed that the metal carbonyls dissociate in the plasma to give rise to positive metal ions, which are then attracted back toward the field emission tip to nucleate and form the metallic needles. The electron avalanche sustains the plasma.

By limiting the growth field-emission current to values of typically a few hundred nanoamps, single nanowires can be grown.<sup>15</sup> While the nanowires bear a resemblance to some of the smaller dendritic "needles" earlier reported, it is not clear that they originate from the same growth regime. In the growth of single nanowires, a similar mechanism is thought to take place, but with important differences as the growth parameters are quite different. Most significantly, the growth currents used are much lower, and the anode to cathode distance is considerably shorter than the mean free path of the precursor molecules and, hence, cannot sustain a glow discharge. The ability to grow single nanowires, as opposed to massive growth of dendrites, allows us to characterize and study the growth process in detail.

This paper concerns our preliminary studies on the mechanism underlying the growth of nanowires induced by field emission. Although there are several mechanisms at play, we believe the primary mechanism to be direct deposition of metal ions. The focus of this paper will be on the primary mechanism of growth, but we will also discuss alternate growth mechanisms that influence the formation of the nanowires. We present some direct evidence of the primary mechanism. To demonstrate the primary growth mechanism, we had chosen the growth of tungsten nanowires from tungsten carbonyl as it demonstrates minimal secondary effects. We will also present examples of other growth mechanisms involved.

TABLE I. Precursors for nanowire growth.

Nanowire material	Precursor
Tungsten	Tungsten hexacarbonyl
Iron	Iron pentacarbonyl
Cobalt	Dicobalt octacarbonyl, cobalt tricarbonyl nitrosyl
Carbon	Benzene, naphthalene, acetylene
Silicon-carbon	Tetramethyl silane

## II. EXPERIMENTAL PROCEDURE

The experimental setup is installed in the specimen chamber of a scanning electron microscope (Philips XL30 ESEM FEG), as shown in Fig. 1. The base pressure in the chamber is better than  $3 \times 10^{-6}$  mbar, while the local precursor vapor pressure at the delivery nozzle is estimated from the chamber pressure during growth and the pumping speed of the system. A nanomanipulator is used to position the positively biased anode in the vicinity of the growth initiation point. The current in the circuit is controlled by a high-voltage source-measurement unit (SMU) with a voltage compliance set at 1 kV or lower. Growth is initiated by field emission from a pointed structure, such as a vertical carbon nanotube, an etched tungsten tip, or a similarly shaped nanostructure. Alternatively, for microscopically flat surfaces, a nanowire can be initiated through an arc discharge by touching the surface with the anode, and breaking the contact under constant current control. Unfortunately, this technique damages the surface. A more controlled method uses tunneling induced growth of a nanodeposit<sup>29</sup> on the surface from which field emission can then take place. However, this is not normally carried out due to the difficulty in controlling the tunneling process with the existing nanomanipulators.

Nanowires have been grown using the same technique from the precursors listed in Table I. The growth from these precursors exhibits vastly different physical characteristics, suggesting that more than one mechanism could be at play. Iron pentacarbonyl gives rise to thin iron nanowires with core diameters of about 20 nm [Fig. 2(a)]. Cobalt tricarbonyl nitrosyl, on the other hand, results in a nanowire with a very thin initial growth followed by rapid thickening. Acetylene results in carbon nanowires with a corrugated surface [Fig. 2(b)], while those grown from benzene are smooth and conical in shape. Of all nanowire growth, nanowires from tungsten carbonyl showed the most controlled growth behavior with no dramatic changes as growth current is increased. Therefore, it was chosen as the primary subject of our study.

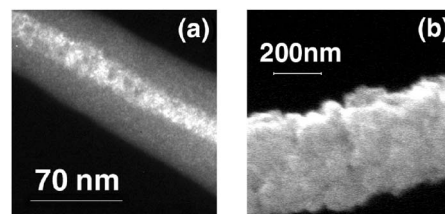


FIG. 2. (a) Dark-field TEM image showing typical iron nanowire with a core diameter of about 20 nm. (b) SEM micrograph of a carbon nanowire with corrugated surface grown from acetylene.

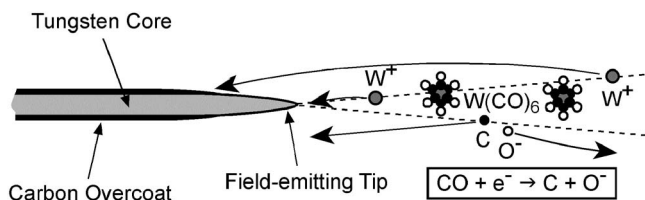
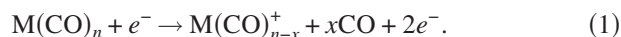


FIG. 3. Schematic of dissociation processes near the growing nanowire tip. The dashed line illustrates the cone of electrons emitted from the tip. Neutral carbon atoms intercepted by the wire form the amorphous overcoat.

### III. GROWTH MECHANISM

The proximity of the anode to the cathode, typically between 1–100 microns, is much less than the mean free path of a few millimeters for gas molecules at 0.01 mbar (estimated pressure at the gas delivery nozzle). This reduces significantly the likelihood of forming secondary ions and electron avalanches that is characteristic of a glow discharge. In this situation, most of the ions are formed by direct electron impact from the field-emitted electrons. In the formation of a nanowire through this mechanism, we need to consider the interaction of the field-emitted electron with the precursor molecule, the trajectory of the products of the interaction, and the processes involved in the deposition and growth of the nanowire.

The dissociation of metal carbonyl molecules [Eq. (1), where  $M$  is the metal] by electron impact to form partially stripped carbonyls and carbon monoxide is fairly well established using mass spectrometry.<sup>30</sup>



For tungsten carbonyl, the minimum energy required to remove a single carbonyl molecule is about 8.47 eV. Due to the high electric fields required for field emission, the field-emitted electrons would reach such energies beyond a distance of a few tens of nanometers from the tip. The energy requirements for other metal carbonyls are similar. Since the partially stripped carbonyl is positively charged, it will be further bombarded by electrons along its trajectory to the tip. Further dissociations of a partially stripped carbonyl require significantly less energy.<sup>31</sup>

From simulations of ions formed during field emission, only those very near the tip will eventually land on the tip.<sup>32</sup> There is a difference, however, in that the fragments from dissociated carbonyl molecules will have higher kinetic energy compared to purely ionized gas molecules.<sup>33</sup> Our trajectory simulations show that ions formed a few tens of nanometers away from the nanowire land on the tip, whereas ions from further away tend to land on the shank (Fig. 3). Studies of direct ion beam deposition of metals show that the sticking coefficient is near unity for energies in the range of a few tens of electron volts.<sup>34</sup> Higher ion energies result in self-sputtering. Since the returning metallic ions are mostly singularly charged, the ion energies are no more than a few tens of electron volts and have a high probability of sticking upon landing.

Unlike the needles grown by Okuyama *et al.*,<sup>24</sup> where only trace amounts of carbon were found within the needles, our single nanowires have a thin carbonaceous coating. TEM

observations show two carbonaceous layers, a denser core and a lighter outer coating. The outer coating is contamination formed while imaging; whereas, the inner carbonaceous shell originates from the growth process.

We propose that the carbonaceous layer originates from dissociative attachment of the CO molecule from electron bombardment (Ref. 33, p. 418):



The  $\text{O}^-$  ions will be attracted toward the anode and will not influence the growth. The resulting carbon then condenses on the substrate. The carbon formed is not charged and, therefore, is not influenced by the electrostatic field to focus it on to the tip. The carbon that intercepts the nanowire simply overcoats it.

#### A. Experimental evidence

We had previously observed that while it was possible to grow nanowires of different materials by changing the precursors, the resultant nanowires tend to have differing diameters. In our previous work,<sup>15</sup> we noticed that while it was easy to grow a thin nanowire on a thicker one, the reverse, growing a thick nanowire on a thin nanowire, is a difficult process. We had also observed that if the nanowire is bent at an angle, the thickening process stops at the elbow and does not proceed further down the shank of the nanowire. This observed behavior provides direct evidence for the ion trajectory deposition model of nanowire growth. The following experiment was performed to investigate this mechanism of growth.

Initially  $\text{W}(\text{CO})_6$  is introduced into the chamber and a field emission current of 1  $\mu\text{A}$  is used to grow several thin and short tungsten nanowires for 2 min. The current is then increased to 5  $\mu\text{A}$  for 30 s to thicken and strengthen these nanowires. This provides long slender tungsten nanowires of about 3  $\mu\text{m}$  in length [Fig. 4(a)] (step 1). In the second part of the experiment,  $\text{W}(\text{CO})_6$  is replaced by tetramethyl silane  $[(\text{CH}_3)_4\text{Si}]$ . The growth is continued at 5  $\mu\text{A}$  to grow silicon-containing nanowires, and a picture is taken every 1 min (step 2). After satisfactory growth and thickening has been achieved, the growth is continued with  $\text{W}(\text{CO})_6$  at 1  $\mu\text{A}$  for 10 s and 5  $\mu\text{A}$  for another 10 s to initiate forking. This results in fine tungsten nanowires with multiple forks grown on the previous structure. The forks caused the subsequent nanowires to form at an angle to the original nanowire (step 3). The precursor source is then switched back to  $(\text{CH}_3)_4\text{Si}$  and growth is continued at 5  $\mu\text{A}$  to thicken the nanowires [Fig. 4(b)] (step 4). The progression of the nanowire growth is illustrated in Fig. 5.

The difference in nanowire diameter for different precursors is largely determined by the radial velocity distribution of the returning ions that is highly dependent on the growth conditions and the precursor used. Circumstances that influence the distribution profile include the distance at which the ions are generated, the initial kinetic energy of the ionized fragments, and the electrostatic field surrounding the tip of the nanowire. Smaller radial velocities mean that ions generated near the field-emitted electron beam axis would return

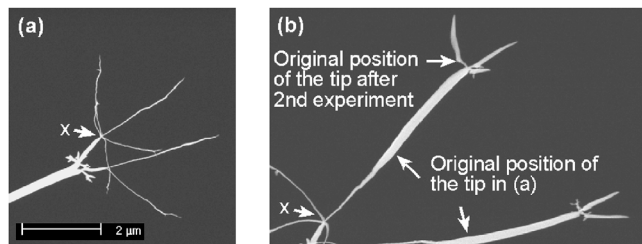


FIG. 4. Multiply forked tungsten nanowires. (a) After step 1, and (b) after step 4 (see text). The thicker portions result from overcoating using tetramethyl silane precursor. The point labeled “X” refers to the same point in (a) and (b).

close to the axis and favor the growth of a thin nanowire. When a thicker nanowire is being grown on a thin nanowire, most of the returning ions miss the tungsten nanowire tip “target” and fly past the tip. However, there is still a radial electric field component at the shank to attract the ions to land on the shank.

The first part of the experiment (step 2) shows that the returning ions slowly coat the tungsten wire while slowly increasing its length. The profile of the coated wire thickens toward the tip, consistent with the theory that growth is caused by returning ions as the ions will first coat the tip. As the coating increases in thickness, it shields the lower part of the wire from further growth. The experiment shows that the thickening can happen along a stretch of nanowire extending  $3 \mu\text{m}$  behind the tip, suggesting that the ions are capable of traveling at least  $3 \mu\text{m}$  beyond the tip. However, in the case of the short nanowires with elbows, the thickening stops abruptly at the elbow. If field induced decomposition<sup>29</sup> were primarily responsible for this growth, the silicon layer would be unable to coat the shank of the tungsten wire, and the growth of the silicon nanowire would begin abruptly at the end of the tungsten nanowires. If thermal decomposition had been the dominant mechanism, it would have been able to coat past the elbow. This abrupt discontinuity in thickness could only have been possible if growth was caused by returning silicon ions missing the tungsten nanowires and flying past the elbow of the wire. Growth of nanowires at high currents on planar surfaces gives rise to a deposited disk on the substrate centered on the nanowire base. This is caused by the returning ions that missed the shank of the nanowire and eventually landed on the surface.

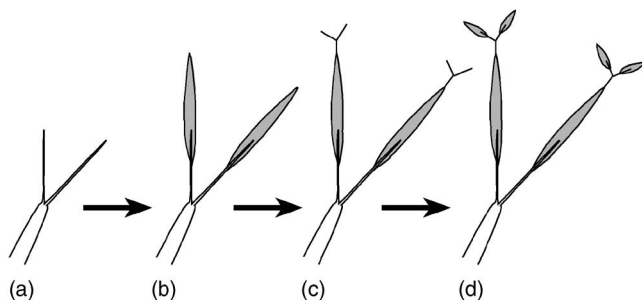


FIG. 5. Schematic of experiment. (a) After step 1, (b) step 2, (c) step 3, and (d) step 4. The gray shaded areas represent material deposited using a tetramethyl silane precursor.

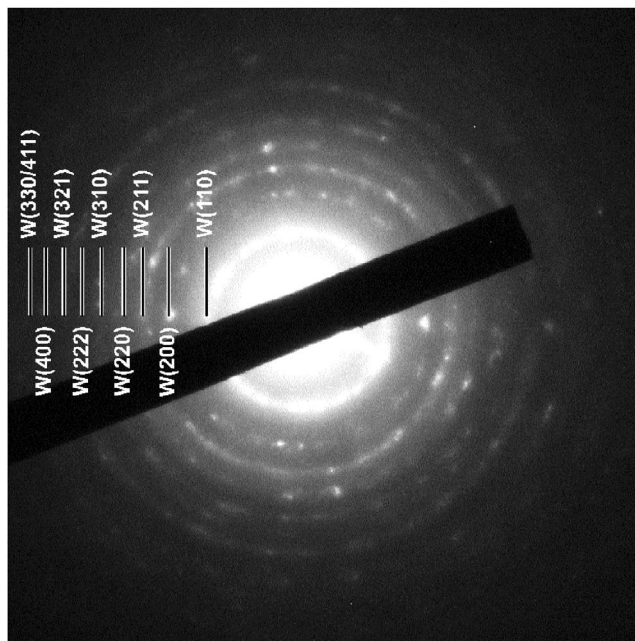


FIG. 6. Typical selective-area diffraction pattern of nanowires grown from  $\text{W}(\text{CO})_6$  precursor, indexed with most probably  $(hkl)$  planes.

## B. Structural analysis and phase identification

Okuyama *et al.*<sup>25,27</sup> had reported on the observation of nonstandard crystalline phases with expanded lattice constant in Mo,<sup>27</sup> and fcc structure in Cr,<sup>25</sup> for needles grown by corona discharge. Such unusual structures were attributed to the high stress due to the electric field during growth. Electron diffraction patterns of W needles were, however, not remarkable. Needles grown at room temperature were typically made up of unoriented crystallites.<sup>28</sup> Chemical analysis on Cr and Mo needles was carried out by Auger electron spectroscopy (AES), and indicated the presence of trace amounts of carbon possibly incorporated into the needle during growth. Varying amounts of oxygen were found on the needles’ surface regions, depending on the growth conditions. Unfortunately, we are not aware of any studies that have been conducted on the presence of O and C species in the bulk of such needles. Such information may allow us to estimate the possibilities of O and C incorporation in the bulk of our nanowires, thereby allowing us to correlate with the electrical properties of our nanowires.

Moreover, the growth field-emission current for single nanowire growth is very much lower than those encountered in corona-discharge growth; therefore, the morphological and structural features are not known. In the present study, selected area electron diffraction (SAED) was carried out to determine the structure and phase of tungsten nanowires grown at currents ranging from 20 to 1000 nA. Attempts to determine the presence of second phases comprising W, C, and/or O were also carried out via SAED. High-resolution TEM imaging was carried out using a Philips CM300 and a JEOL JEM-3010, both operating at 300 keV. The results of these investigations are presented below.

Figure 6 shows an indexed selected area diffraction pattern (SADP), which is typical for tungsten nanowires grown at all growth currents. Figure 6 clearly shows that all tung-

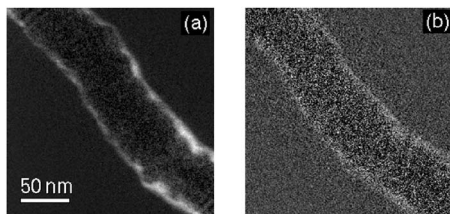


FIG. 7. Energy-loss images of nanowires grown from  $W(CO)_6$  precursor, depicting the spatial distributions of (a) carbon, and (b) oxygen.

sten nanowires have unexpectedly high crystallinity despite their rapid growth rate ( $\sim 2500$  nm/min) and ambient temperature at which nanowire growth was conducted. Moreover, equilibrium bulklike bcc crystal structure was detected for all specimens grown at all growth currents with no detectable lattice expansion. This result led us to the possible implication that sources of energy other than resistive heating (which we believe is minimal) may be available for enhanced atomic diffusion, thereby enabling reconstruction and grain growth and/or coalescence to occur. The possible sources of thermal energy are (a) enhanced phonon scattering with the surfaces and grain boundaries of wires with nanometer dimensions and (b) energetic and repeated impact of returning  $W^+$  ions onto nanowire growth front that is rapidly evolving during the growth process. While the former is a typical thermal energy source available for nanostructured materials, the latter is unique to the field-emission induced growth process and is believed to be the major thermal source leading to high crystallinity of the nanowires. The absence of elongated lattice parameters is probably due to the numerous crystalline defects and dislocations that might have fully compensated for the localized lattice elongations. Our suspicion was later confirmed by TEM dark-field images and will be discussed later.

The presence of C and O in the organometallic precursor raised concerns about the chemical homogeneity of as-grown nanowires. As such, SAED was undertaken at various parts of tungsten nanowires grown at different currents. All our SADPs exhibit no systematic correspondence with those of WC,  $W_2C$ , and  $WO_3$ , thereby confirming that there exists no detectable crystalline second phase particles within the cylindrical tungsten core. These results demonstrate the capacity of field-emission induced growth to fabricate tungsten nanowires of high phase homogeneity at ambient growth condition.

Examination of the SADPs reveals a broadening of the Debye-Scherrer rings as the growth current decreases, showing that the mean grain size of the tungsten nanowires generally increases with growth current. This observation is consistent with those obtained via TEM dark-field imaging and will be discussed later.

### C. Chemical compositional analysis

In order to determine the chemical nature of the nanowires, attempts were made to study as-grown specimens via electron energy loss mapping and imaging. Unfortunately, nanowires of smaller diameters (growth current  $< 500$  nA) suffered from severe vibration in the electron beam. Thus,

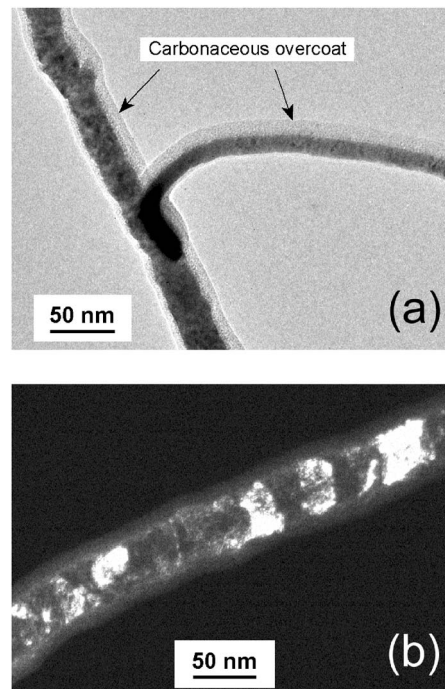


FIG. 8. (a) Image of a nanowire at a branch junction. The overcoat is thickest on the side facing the growing tip front that is located beyond the top of the image. The underside of the branch has almost no overcoat. (b) Typical dark-field image of tungsten nanowire. Regions of strong diffraction contrast are observed in all portions of the nanowire, while the carbonaceous overcoat exhibits diffused scattering.

we have restricted our core-loss imaging studies to nanowires grown at 500 nA. The results are believed to be representative for specimens grown at lower currents. The results of our energy-loss imaging are depicted in Fig. 7.

The core regions of as-grown nanowires comprise mainly tungsten with trace amounts of C and O. A strong C-loss signal [Fig. 7(a)] is detected in the coating enveloping the nanowire and confirms the carbonaceous nature of the outer coat. Figure 7(a) also clearly demonstrates the spatial distribution of C atoms in the outer coat formed during the nanowire growth, thereby offering strong evidence supporting the proposed mechanism of nanowire formation. The oxygen map [Fig. 7(b)] shows only small traces of oxygen in the carbon coating surrounding the nanowire. As such, we believe the amount of oxygen present in as-grown specimens is negligibly small. The oxygen  $K$  edge in the electron-energy-loss spectrum acquired in the same region of the specimen reassures us that little oxygen is present. In conclusion, electron-energy-loss spectroscopy (EELS) analysis confirms the elemental nature of the core and outer coat of as-grown nanowires. The spatial distributions of these elements lend support to our proposed field-emission induced growth mechanism. Unfortunately, the carbonaceous coat needs to be selectively removed in order to fully ascertain the absence of C and O species in the nanowire core regions. Attempts to remove the overcoat and EELS studies are underway and will be discussed elsewhere.

### D. Morphological analysis

TEM bright-field (BF) imaging was employed to study the dependence of morphology and cross-sectional diameter

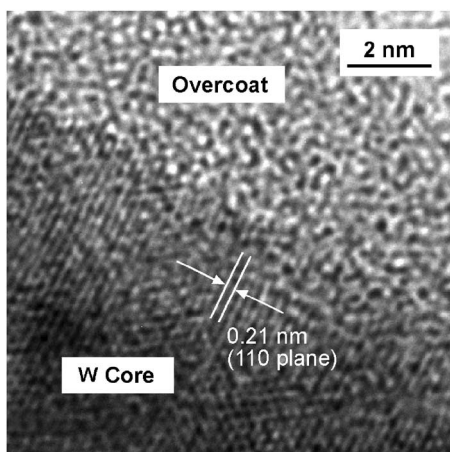


FIG. 9. High-resolution image at the interface between the tungsten core and amorphous overcoat showing the lattice spacing and its corresponding bulk Miller index.

of tungsten nanowires on field-emission current. Figure 8 shows bright-field and dark-field images of tungsten nanowires. Strong diffraction and mass thickness contrast is observed in Fig. 8(a), which shows the existence of two phases of vastly different atomic weight and degree of crystallinity in the specimens. The denser phase (tungsten) constitutes the cylindrical core of quasiuniform diameter; while the less-dense phase is carbonaceous and encapsulates the core. The uniform contrast of the carbonaceous encapsulating layer, in Fig. 8(a), and its characteristic diffuse scattering, seen in Fig. 8(b), suggest that it is amorphous with short range crystalline order. The high electron transparency of the carbonaceous encapsulating layer suggests that it is of amorphous structure with probably localized  $sp^3$  bonding rather than of  $sp^2$  graphitic, layered structure. This is confirmed by our TEM high-resolution phase-contrast images (Fig. 9). The nanowire morphology as depicted in Fig. 8(a) is observed in specimens grown at lower currents. On larger diameter wires (grown at 1000 nA), tapering of the core diameter toward the growth front is clearly observed. The carbonaceous overcoat likewise reduces toward the tip and is not observable at the growth front. Examination of all acquired BF images reveals localized regions of varying diffraction contrast regardless of the growth current value. Nodular particles of different gray levels are also observed in nanowires grown below 1000 nA. Such observation is consistent with the fact that as-grown tungsten nanowires are one-dimensional polycrystalline aggregates with nanosized grains.

Our observations also show the carbonaceous coating to be formed unevenly over the surface, and in many cases, the thickness of the carbonaceous layer is different on opposing sides of the wire diameter [Fig. 8(a)]. This does not support the origin of carbonaceous layer from electron-beam induced contamination during observation, since the layer thickness would have been even throughout. However, such uneven coating would be expected if carbon atoms from the dissociative attachment of CO were to simply coat the nanowire shank. Unlike charged  $W^+$  ions, the trajectories of the neutral C atoms, polarized by the electric field in the vicinity, are only weakly influenced by a nonuniform electric field. The

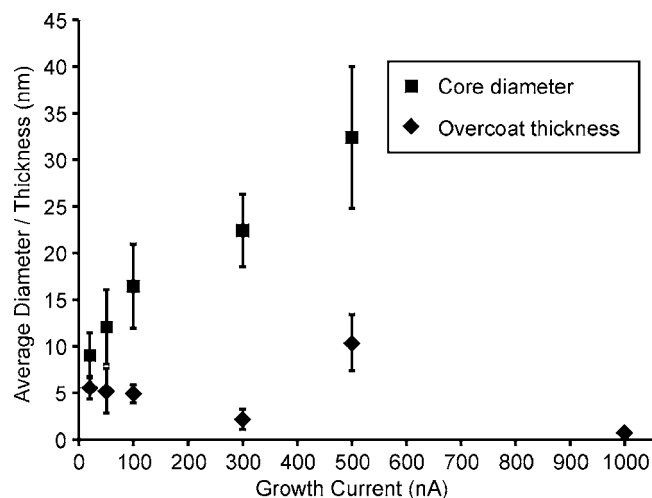


FIG. 10. Average tungsten core diameter and thickness of carbonaceous overcoat of as-grown nanowires vs growth current.

main factor governing the C atom trajectories are the velocity components arising from the dissociative attachment process. Uneven carbonaceous coating is invariably observed where the nanowire is curved, with a thicker coating favoring the side where the emitting tip is located. Indeed, if the wire is sufficiently curved such that one side is out of the line of sight from the growth front, no carbon coating can be discerned on the outer perimeter. Occasionally, some nanocrystals of tungsten with diameters of less than 2 nm embedded in the overcoat were observed. These are believed to have originated from returning  $W^+$  ions formed far ahead of the point where they finally intercepted the nanowire shank.

The presence of the carbonaceous overcoat presents a problem in defining the nanowire diameter. Atomic force microscope (AFM) line scans over nanowires lying on silicon substrates were performed initially to determine the diameter, but such measurements include the overcoat and additional electron-beam induced contamination from inspection of the wire in the scanning electron microscope (SEM). As such, TEM was used as an alternative technique to investigate the metal core diameter dependence on the growth current. Based on numerous acquired BF images, diameter measurements were made at various portions of the nanowires. The average diameter of nanowires grown at various field-emission current is shown in Fig. 10. The tungsten core diameter increases with field-emission current but at a diminishing rate at higher currents and is discussed in Sec. IV. On the other hand, there is no systematic variation of the average carbonaceous coat thickness with field-emission current, consistent with our hypothesis of weak influences of nonuniform electric field on C deposition.

### E. Grain morphology

As the SADPs indicate the polycrystalline nature of tungsten nanowires, the effects of growth current on mean grain size and grain size distribution were studied via dark-field (DF) imaging.

The dark-field image in Fig. 8(b) was formed using the (110) reflection, which is typically observed from all nano-

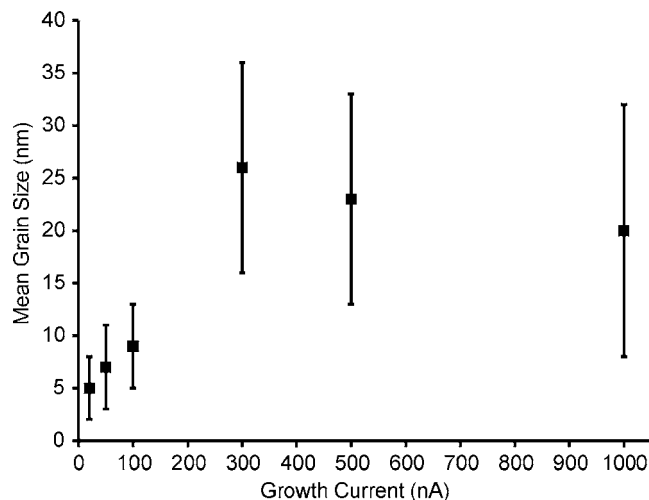


FIG. 11. Average grain size at different growth currents determined via dark-field imaging.

wire specimens. Nanocrystalline grains with diameters of about 20–30 nm are clearly observed in the core region; whereas, the outer coat exhibits diffuse scattering showing that it is without long range crystalline order. Close examination reveals that some dark nodular particles seen in the BF images diffract strongly in the DF images, confirming that they are single nanocrystals. Our DF images also show that these nanocrystallites are irregularly shaped with some of them being columnar. We suspect such columnar morphology may arise from the heat dissipation from the nanowire growth front to the base. For larger-diameter nanowires, two or more grains were found to span the diameter as evidenced from the Moiré fringes in our high-resolution TEM images. We also observed alternating, nonuniform contrast on the length scale of 1.5 nm within a single diffracting crystal (image not shown). This is caused by localized defects such as dislocations that were introduced during the nanowire formation process characterized by high deposition rates.

We have carried out extensive DF imaging using the (110) reflection on various portions of our tungsten nanowires grown under different field-emission current. By measuring the sizes of the diffracting nanocrystals of our specimens in DF image mode, we have attempted to determine the influence of growth current on the average size and size distribution of these nanocrystals. Results of our measurements are shown in Fig. 11. The absolute value of the mean grain size is subject to error due to the uncertainty in the overlap between grains perpendicular to the incident beam. Nevertheless, such systematic error exerts equal influences on all our specimens and, hence, does not affect the variation of mean grain size with field-emission current. It is seen that the average grain size increases with growth current but saturates at around 20–25 nm at 1  $\mu$ A. The range of grain sizes observed also increases with growth current. For small diameter wires grown at low currents, grains are often found to straddle the wire diameter resulting in columnar growth, while large-diameter wires comprise grains with a wide range of size. The high degree of crystallinity in the nanowires suggests a significant amount of energy is available to drive the crystallization process, which is postulated to come

from the energy imparted by the returning ions and the elevated temperature due to Joule heating at the growth front at higher growth currents. The latter's contribution is believed to be relatively insignificant compared to ion bombardment at the growth front. This has been confirmed by high-resolution TEM images (not shown) of W nanowires grown at field-emission currents of 50 nA, which revealed disordered, amorphous structure at the interface between the nanowire and the etched tungsten tip. Moreover, independent experiments using as-grown tungsten nanowires in field-emission studies showed that the nanowire recrystallizes into a long slender single crystal at the apex after a short period of emission.

#### IV. CHARACTERIZATION OF NANOWIRE GROWTH

With the ability to grow single nanowires instead of uncontrolled dendritic growth, it is now feasible to study the growth characteristics. It was observed very early on that the key to controlling the growth of the nanowires lies in the control of the field-emission current. The choice of current determines whether a nanowire grows as a single filament or as multiple branched filaments; it also affects the wire diameter and axial growth rate. It was observed that as current is slowly increased, a nanowire grown on an etched tip evolves from a single nanowire to one with multiple forks.

To study the growth-rate dependency on growth current, nanowires were grown on a substrate by a technique described in Ref. 19. The growths were carried out for 3 min each at a chamber pressure of either  $1 \times 10^{-5}$  mbar or  $5 \times 10^{-5}$  mbar with the vapor admitted. The length of the nanowire was measured by SEM while the diameter determined by AFM, noting that the latter includes the thickness of the carbonaceous overcoat. On thick wires, we found AFM measurements difficult, as the wires are rigid and do not fully contact the surface, thus yielding inconsistent values. Their diameters were determined by SEM instead.

##### A. Axial growth rate

There is a monotonic correlation between growth current and axial growth rate but the relationship is not linear (Fig. 12). At  $5 \times 10^{-5}$  mbar chamber pressure, the nanowire is 10  $\mu$ m long at 30 nA as compared to 30  $\mu$ m at 1  $\mu$ A after growth of 3 min. The diameter of the nanowire is also larger. For a 33-fold increase in current, the length has only increased three times. The growth rate for a specified current shows a reasonably proportional behavior with chamber pressure.

The role of ion bombardment on field-emission tips and its contribution to the formation of noise in field emission is quite well known. The formation of ions is directly proportional to the product of current and pressure.<sup>35</sup> The volume growth rate should follow the same rule if the growth were solely dependent on the ions generated. If there is no change in the angular and spatial distribution of ions landing on the nanowire, there would be no change in the deposition profile, and hence, no change in the nanowire diameter. In such situations, the axial growth rate should increase linearly with growth current.

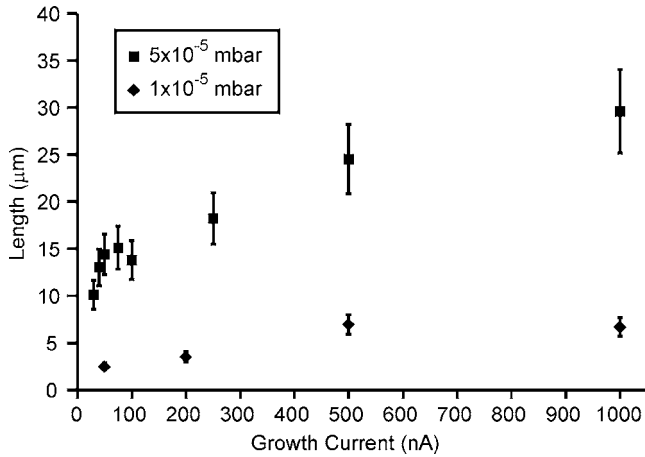


FIG. 12. Nanowire length vs growth current for 3 min growth at 1 and  $5 \times 10^{-5}$  mbar chamber pressures.

Simulations of trajectories of ions formed in the ambient by electron impact during field emission show that only ions generated near a field-emission tip will eventually land on the tip.<sup>32</sup> Ions from further distances will land on the shank. Our simulations show that only ions generated in the volume within a few tens of nanometers away from the nanowire tip will land on the tip of the nanowire. We believe that the current density during field emission in the volume directly ahead of the tip is so high that ionization and attraction of the ions out of that volume depletes the amount of molecules present. There is one significant difference in this situation compared to that experienced by ion bombardment in normal field emission—the ions in field emission growth stick on the surface and condense, whereas ions from normal emission are discharged and returned to that volume. Comparison between axial growth at lower vapor pressures and higher vapor pressures show a proportional dependence (Fig. 12) on vapor pressure. This is consistent with the theory that the growth is vapor-flow supply limited.

The growth dynamics of the nanowire are illustrated in Fig. 13, where the conical boundary shown contains the electron trajectories, with a semiangle of typically a few degrees, from the field-emission tip. No ions are generated by primary electrons in the first few nanometers from the tip, as the electron energy is insufficient for dissociation and ionization of the metal carbonyl. Volume  $V_1$ , which is close to the tip, has a very small surface area because of its small perimeter, and therefore, the rate of replenishment is also correspondingly small. This is further compounded by the fact that most organometallics are heavy molecules with low thermal velocities. When the growth current is increased, the volume  $V_1$  becomes depleted of available target molecules, reducing the amount of ionization per electron significantly. Depletion is less pronounced in volume  $V_2$ , since its larger perimeter ensures the molecules are more quickly replenished, while the electron current density traversing the volume is also lower. Since axial growth primarily results from ions from  $V_1$ , the axial growth rate saturates. The stunted axial growth combined with the increase of ions contributing to radial growth from  $V_2$  causes the nanowire to thicken up.

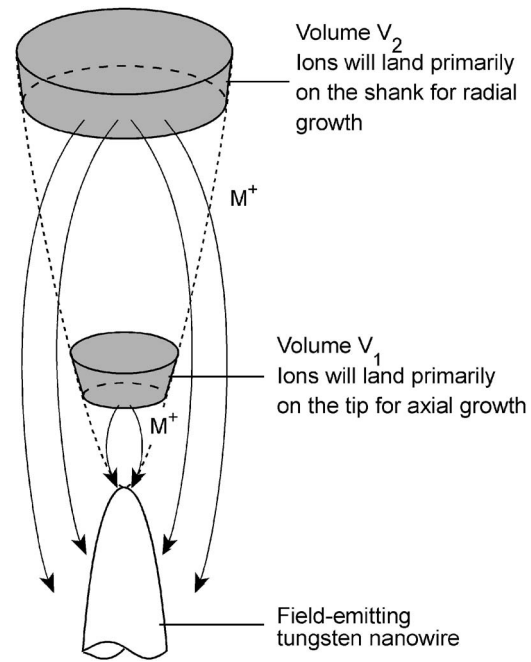


FIG. 13. Schematic showing the relative contributions to axial and radial growth for ions generated close to the emission tip, and those generated further away from the tip.

A simple model of the formation of ions in volume  $V_1$ , and hence the axial growth rate, can be obtained by considering the mass flow in and out of this volume. In a steady-state situation, the rate of molecules entering the volume  $V_1$  ( $N_{in}$ ) must equal the rate of molecules exiting ( $N_{out}$ ) and the rate of molecules being dissociated and ionized ( $N_{ion}$ ):

$$N_{in} = N_{out} + N_{ion}.$$

Therefore,

$$k_1 \rho_0 = k_1 \rho_V + k_2 \rho_V n_e, \quad (2)$$

where,  $k_1$  is the constant dependent on the velocity of the gas molecules;  $k_2$  is the constant dependent on the electron impact cross section of the gas molecule;  $\rho_V$  is the density of molecules inside  $V_1$ ;  $\rho_0$  is the density of molecules outside  $V_1$ , and  $n_e$  is the number of electrons traversing the volume.

Rearranging Eq. (2) to solve for  $\rho_V$ , we obtain:

$$\rho_V = \frac{k_1 \rho_0}{k_2 n_e + k_1}. \quad (3)$$

We assume the axial growth rate to be proportional to the rate of ion formation ( $N_{ion}$ ) and, hence,

$$N_{ion} = \frac{k_2 k_1 \rho_0 n_e}{k_2 n_e + k_1}. \quad (4)$$

Rearranging Eq. (4), we obtain

$$\frac{1}{N_{ion}} = \left( \frac{1}{k_2 \rho_0} \right) \frac{1}{n_e} + \frac{1}{k_1 \rho_0}. \quad (5)$$

Since the axial growth rate of the nanowire is determined primarily by the generation of ions in the volume directly ahead of the tip, the length of the nanowire is proportional to  $N_{ion}$ . Therefore, a plot of reciprocal length

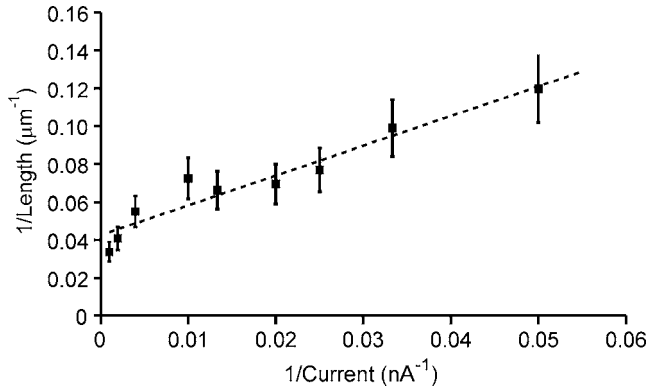


FIG. 14. Plot of reciprocal length vs reciprocal growth current using the data from Fig. 13 for growth at  $5 \times 10^{-5}$  mbar chamber pressure.

against reciprocal current should yield a linear relationship. Figure 14 shows the data from Fig. 12 replotted to determine the relationship. Although there is quite a bit of scatter, the fit is reasonable, suggesting that the proposed mechanism is possible.

We consider, for instance, the nanowire grown at  $1 \mu\text{A}$ . We assume a simplified situation where the electrons leave the tip of the nanowire with trajectories parallel to the axis and contained within a cylinder of diameter ( $d$ ) 10 nm near the tip. A simple estimate can be made of the ratio of the number of ions formed to the number of molecules entering based on our experimental values. The rate of molecules entering the cylinder (per unit length) is given by

$$N_{\text{in}} = \frac{\bar{v} \pi d \rho_0}{4},$$

where  $d$ =diameter of cylinder (10 nm),  $\bar{v}$ =mean velocity of the molecules [ $12.5 \times 10^3 \text{ cm s}^{-1}$  for  $\text{W}(\text{CO})_6$  at 300 K]. The rate of ions formed per unit length ( $N_{\text{ion}}$ ) is given by

$$N_{\text{ion}} = \sigma n_e \rho_V,$$

where  $n_e = 6.24 \times 10^{12}$  electrons/s at  $1 \mu\text{A}$ , and  $\sigma$ =typical value of electron impact cross section for  $\text{W}(\text{CO})_6$  ( $2 \times 10^{-16} \text{ cm}^2$ ). The ratio of molecules being ionized to the molecules entering is thus

$$\frac{N_{\text{ion}}}{N_{\text{in}}} = \frac{4 \sigma n_e \rho_V}{\bar{v} \pi d \rho_0} = \left( 1 + \frac{\bar{v} \pi d}{4 \sigma n_e} \right)^{-1}.$$

The ratio of ions formed to the number of molecules entering is 0.56. The rate of ion formation is thus of the same order as the rate of molecules entering. Therefore, it is not surprising that the axial growth rate shows saturation caused by limited vapor supply.

## B. Volumetric growth rate

As previously mentioned, the diameter of the nanowires increases with increasing growth current. The number of ions formed and, therefore, the volume of material formed should be dependent on the product of the current and pressure. However, our results show a volumetric growth rate that is higher than expected with increasing current. Since the volume of material grown is proportional to the number of ions

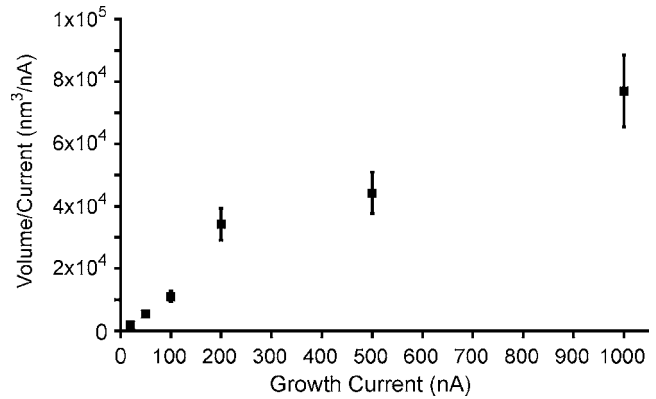


FIG. 15. Growth volume for 3 min growth, normalized by the growth current. Error in estimation primarily arises from the uncertainty in the overcoat thickness.

formed, the ratio of the volume of material formed and the growth current should be constant. A plot of (volume/current) versus current (at constant vapor pressure) shows an increasing ratio as the current is increased (Fig. 15). For example, the amount of material generated per unit current at  $1 \mu\text{A}$  is approximately eight times that at 100 nA.

An increase in the current *per se* does not result in an increase in the efficiency of ion formation, but an increase in electron energy improves the ion generating efficiency. Ion generating efficiency tends to peak at electron energies about 100 eV and decline gradually after that. We believe the increased growth rate is caused by the increase in anode voltage due to the increased nanowire diameter and tip radius (and, hence, poorer electric field enhancement factor). Typical anode voltages for growth of nanowires at low currents ( $\sim 100 \text{ nA}$ ) are about 50–100 V, whereas thicker nanowires ( $\sim 1 \mu\text{A}$ ) need about 200–400 V. This concept is illustrated in Fig. 16.

## V. FORKING PHENOMENON

We had previously observed that in the growth of the nanowires on etched tungsten tips, lower growth currents

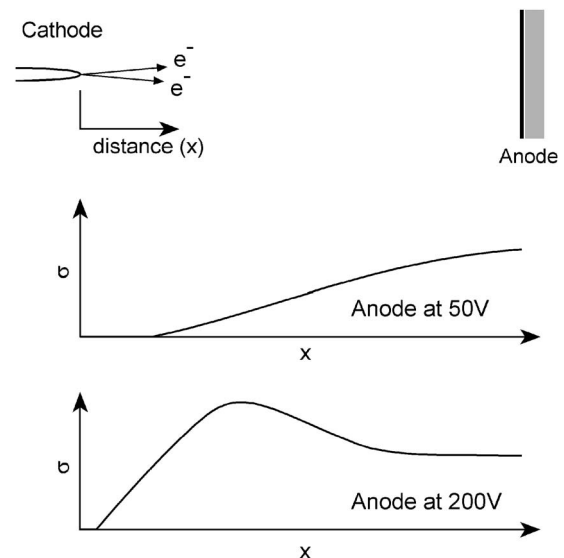


FIG. 16. Illustration of electron impact ionization cross section  $\sigma$  along the space between the cathode and the anode for anode voltages of 50 and 200 V.

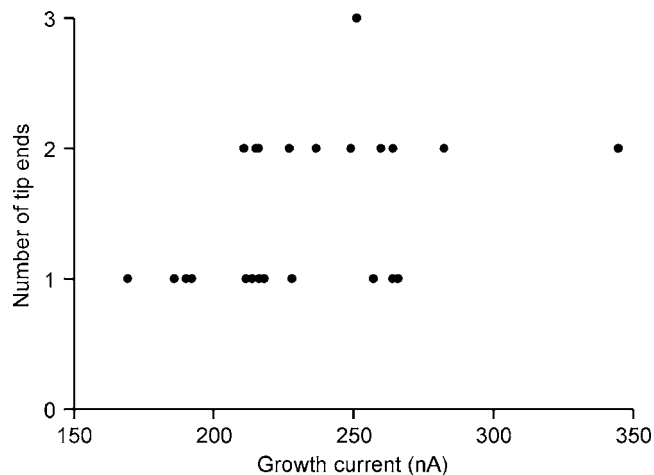


FIG. 17. Number of tips observed to initiate and grow at different currents for a series of repeated experiments.

give rise to smaller nanowire tree structures with fewer forked branches. Further lowering of the growth current ( $<1 \mu\text{A}$ ) results in growth of a few nanowires or a nanowire which forks into a few nanowire branches at its end. If the current used is low enough ( $\sim 100 \text{ nA}$ ), only a single nanowire is formed. This phenomenon is discussed in our earlier publication.<sup>15</sup>

To study this phenomenon, growth was carried out at various growth currents. The number of nanowire tip ends and average growth current was then noted. The nanowire was then melted by heating the etched tungsten tips and the experiment repeated. The scatter plot (Fig. 17) shows a strong positive correlation between the current and the number of tip ends observed. Low currents ( $<100 \text{ nA}$ ) almost consistently resulted in single nanowire growth at the chamber pressure of  $1 \times 10^{-5} \text{ mbar}$ , whereas the higher the current, the higher the probability the tip will result in multiple forked ends. Our experiments also show that nanowires grown on blunt tips are less likely to fork. This is attributed to the way the equipotential surface wraps around the tip. Subsequent experiments show that in growths from flat surfaces, the tip rarely forks, even with currents up to  $1 \mu\text{A}$ ; however, many small branches that appear to be incipient forks are found instead (Fig. 18). The presence of these branches suggests that forks had been initiated, but further

growth of the branches was halted. The number of side branches per  $10 \mu\text{m}$  of nanowire was determined from TEM images of nanowires grown at various currents. Up to around  $100 \text{ nA}$  growth current, no branches were found. Beyond this, the number of branches increases linearly from 2 branches at  $300 \text{ nA}$  to 6 branches at  $1 \mu\text{A}$ . The forking phenomenon is related to the difference in growth rate at different currents. When a fork or branch occurs during nanowire growth, two nanowire ends are formed. Since the system is operated in constant current mode, the two sibling nanowires will compete for the “right to field emit.” The longer nanowire experiences a higher electric field at its tip and will now emit most of the current, inevitably reducing the growth of its shorter sibling nanowire. This effect, in addition to electrostatic screening by the longer nanowire suppresses the growth of the shorter sibling nanowire.

We believe that the lack of forking at low currents ( $<100 \text{ nA}$ ) as compared to higher currents is due to the larger difference in growth rates at low currents. From Fig. 12, the growth rates and corresponding currents are  $2.8 \mu\text{m}/\text{min}$  at  $20 \text{ nA}$ ,  $4.8 \mu\text{m}/\text{min}$  at  $50 \text{ nA}$ , and  $6 \mu\text{m}/\text{min}$  at  $250 \text{ nA}$ . In a hypothetical situation with a growth current of  $70 \text{ nA}$  on a forked nanowire, let us assume that the current is split between the two nanowire ends at  $20 \text{ nA}$  on one end and  $50 \text{ nA}$  the other. The growth rate of the nanowire end at  $50 \text{ nA}$  is  $71\%$  higher than the end at  $20 \text{ nA}$ . However if the growth current is  $300 \text{ nA}$  and is split between the two nanowire ends at  $50 \text{ nA}$  and  $250 \text{ nA}$ , the difference in axial growth rate between the two ends is only  $25\%$ . In the growth at  $70 \text{ nA}$  scenario, the higher growth rate of the  $50 \text{ nA}$  tip will cause it to increase in length more rapidly and eventually all the current will be from that end. The shorter nanowire ( $20 \text{ nA}$  end) will cease to emit and grow. The difference in growth rates for the  $300 \text{ nA}$  scenario would be less and the nanowire end at  $50 \text{ nA}$  has a better chance of continued growth. In addition, the nanowire at higher currents will become thicker and inevitably reduce its own emission current. Growth at low currents ( $<100 \text{ nA}$ ) tends to encourage domination by one of the nanowires and incipient forks are thus suppressed. Growth at higher currents is more likely to achieve a state that will allow for continued growth of multiple tip ends.

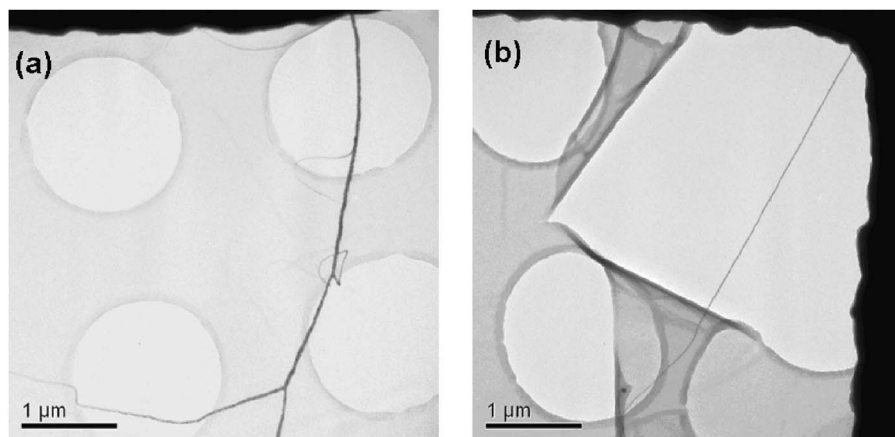


FIG. 18. TEM images showing typical branching morphology of nanowires grown at (a) currents greater than  $300 \text{ nA}$ , and (b) currents below  $100 \text{ nA}$  with little evidence of branching.

## VI. ALTERNATE GROWTH MECHANISMS

In Sec. III, we established that growth by returning ions is one of the major mechanisms in the formation of the nanowire. However, observations of growth from cobalt tricarbonyl nitrosyl  $[\text{Co}(\text{CO})_3\text{NO}]$  show a thin base with a rather thick top. Unlike tungsten nanowires, iron nanowires are also found to have kinks and bends along the nanowire that could not be accounted for by the above theory. These suggest that more than one mechanism may be involved in the formation of the nanowire during growth depending on the precursor used and growth temperature. Thermal decomposition also has a significant role to play in growth of nanowires from  $\text{Fe}(\text{CO})_5$  and  $\text{Co}(\text{CO})_3\text{NO}$ .

When the experiment of Sec. III A was repeated using  $\text{Co}(\text{CO})_3\text{NO}$  instead of  $(\text{CH}_3)_4\text{Si}$ , the result was very different. A thin nanowire was originally grown using  $\text{W}(\text{CO})_6$  at 100 nA, then the current was increased to 500 nA to cause it to fork. Growth was then continued using  $\text{Co}(\text{CO})_3\text{NO}$  with the growth current gradually increased from 100 to 500 nA. The tungsten nanowire becomes coated as in the previous case, but the coating extends past the fork. As opposed to the previous case, these processes tend to happen very fast, quite often within a few seconds compared to a few minutes when  $(\text{CH}_3)_4\text{Si}$  was used. In another experiment, the tungsten nanowire is first grown, followed by a short admission of  $\text{Co}(\text{CO})_3\text{NO}$ , before continuing with tungsten nanowire growth. The wire was then brought to contact the anode. Upon passing a current through the nanowire in a  $\text{Co}(\text{CO})_3\text{NO}$  ambient, a bulge of cobalt deposit was formed at the middle, where the intermission had taken place.

$\text{Fe}(\text{CO})_5$  and  $\text{Co}(\text{CO})_3\text{NO}$  have been known to exhibit autocatalytic growth.<sup>36,37</sup> It was discovered that  $\text{Fe}(\text{CO})_5$  decomposes catalytically on iron lines at much lower temperatures (125 °C) than on silicon (250 °C). It is proposed that the returning cobalt ions overcoat the tungsten nanowire to form a thin seed layer. Joule heating from the electrical current passing through the nanowires during field emitting causes catalytic thermal decomposition of the precursor and deposits cobalt along the tungsten wire. The thickening of the wire reduces the current density and improves the thermal conduction, reducing the temperature gradient along the nanowire until a steady state is reached. The thermal decomposition of  $\text{Co}(\text{CO})_3\text{NO}$  takes place at a particularly low temperature, and the result of this is that attempts to grow cobalt nanowires via field-emission induced growth invariably give rise to rapid growth of thick cobalt wires beyond lengths of several 100 nm. The initial growth remains thin only close to the starting point as thermal conduction keeps the temperature over this length below the threshold for thermal decomposition (Fig. 19).

## VII. CONCLUSIONS

The ability to grow single nanowires has allowed us to study the growth characteristics of metallic nanowires from organometallic precursors by a field-emission induced process, which has hitherto not been possible due to uncontrolled dendritic growth at higher currents. The role of returning metal ions to the growth of the nanowire was

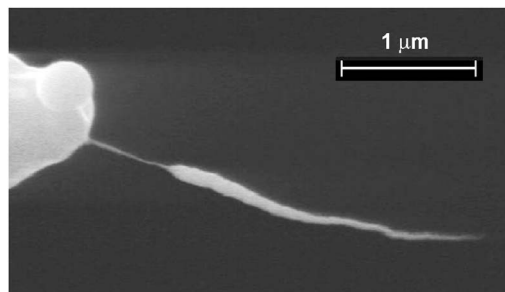


FIG. 19. Nanowire grown from  $\text{Co}(\text{CO})_3\text{NO}$  at 50 nA shows a thin wire at the base growing to a thick bulge toward the tip.

demonstrated experimentally. On the other hand, the carbonaceous overcoat that accompanies such growth is believed to be due to dissociated neutral carbon atoms, which are polarized and weakly attracted to the nanowire by the local non-uniform electric field. Evidence for this comes from the directional nature of the overcoating process, with deposition favoring the side of the nanowire facing the growing field-emitting tip. TEM analysis of tungsten nanowires thus grown shows that the core is largely metallic and is polycrystalline in nature. For nanowires of small diameter, a columnar grain morphology is evident, but as the wire diameter increases, multiple grains span the diameter. The latter leads to a wide distribution of grain size. The axial and radial growth rates of tungsten nanowires as a function of growth current were studied and can be accounted for by assuming a situation in which the rate of ion formation just ahead of the growing tip is supply-rate limited. At higher growth currents, forking (during initiation) and branching (during steady state wire growth) was found to be increasingly probable, and hence, a key to the growth of single, well-defined nanowires, is to keep the growth current low. For growth from tungsten carbonyl, growth currents below 100 nA avoid the formation of side branches. The thermal decomposition of the precursor can also contribute to nanowire growth, and evidence for this mechanism was found in the cases of  $\text{Fe}(\text{CO})_5$ , and  $\text{Co}(\text{CO})_3\text{NO}$ , where autocatalytic decomposition is known to result in metal deposition at relatively low temperatures.

## ACKNOWLEDGMENTS

The authors would like to thank G. F. You and K. S. Yeong who helped to grow the tungsten nanowires for TEM characterization, and Dr. M. Yeadon for his help in interpreting the TEM data. This project was partially funded by a research grant from A\*STAR.

<sup>1</sup>Y. Xia *et al.*, *Adv. Mater.* (Weinheim, Ger.) **15**, 353 (2003).

<sup>2</sup>S. Iijima, *Nature* (London) **354**, 56 (1991).

<sup>3</sup>A. M. Morales and C. M. Lieber, *Science* **279**, 208 (1998).

<sup>4</sup>M. Saito, M. Kirihara, T. Taniguchi, and M. Miyagi, *Appl. Phys. Lett.* **55**, 607 (1989).

<sup>5</sup>T. M. Whitney, J. S. Jiang, P. C. Searson, and C. L. Chien, *Science* **261**, 1316 (1993).

<sup>6</sup>C. R. Martin, *Science* **266**, 1961 (1994).

<sup>7</sup>B. H. Hong, S. C. Bae, C. W. Lee, S. Jeong, and K. S. Kim, *Science* **294**, 348 (2001).

<sup>8</sup>M. P. Zach, K. H. Ng, and R. M. Penner, *Science* **290**, 2120 (2000).

<sup>9</sup>M. Knez, A. M. Bittner, F. Boes, C. Wege, H. Jeske, E. Maiss, and K. Kern, *Nano Lett.* **3**, 1079 (2003).

- <sup>10</sup>Y. Huang, X. Duan, Q. Wei, and C. M. Leiber, *Science* **291**, 630 (2001).
- <sup>11</sup>P. A. Smith, C. D. Nordquist, T. N. Jackson, and T. S. Mayer, *Appl. Phys. Lett.* **77**, 1399 (2000).
- <sup>12</sup>C. Bower, W. Zhu, S. Jin, and O. Zhou, *Appl. Phys. Lett.* **77**, 830 (2000).
- <sup>13</sup>Y. Zhang *et al.*, *Appl. Phys. Lett.* **79**, 3155 (2001).
- <sup>14</sup>C. Cheng, R. K. Gonela, Q. Gu, and D. T. Haynie, *Nano Lett.* **5**, 175 (2005).
- <sup>15</sup>J. T. L. Thong, C. H. Oon, M. Yeadon, and W. D. Zhang, *Appl. Phys. Lett.* **81**, 4823 (2002).
- <sup>16</sup>C. H. Oon, J. T. L. Thong, Y. Lei, and W. K. Chim, *Appl. Phys. Lett.* **81**, 3037 (2002).
- <sup>17</sup>A. B. H. Tay and J. T. L. Thong, *Appl. Phys. Lett.* **84**, 5207 (2004).
- <sup>18</sup>A. B. H. Tay and J. T. L. Thong, *Rev. Sci. Instrum.* **75**, 3248 (2004).
- <sup>19</sup>C. H. Oon and J. T. L. Thong, *Nanotechnology* **15**, 687 (2004).
- <sup>20</sup>H. R. Schulten and H. D. Beckey, *Org. Mass Spectrom.* **6**, 885 (1972).
- <sup>21</sup>H. B. Linden, E. Hilt, and H. D. Beckey, *J. Phys. E* **11**, 1033 (1978).
- <sup>22</sup>F. Okuyama, T. Shibata, and N. Yasuda, *Appl. Phys. Lett.* **35**, 6 (1979).
- <sup>23</sup>F. Okuyama, *Appl. Phys. Lett.* **36**, 46 (1980).
- <sup>24</sup>F. Okuyama, *J. Cryst. Growth* **49**, 531 (1980).
- <sup>25</sup>F. Okuyama, *J. Appl. Phys.* **53**, 6226 (1982).
- <sup>26</sup>F. Okuyama, *Jpn. J. Appl. Phys., Part 1* **22**, 245 (1983).
- <sup>27</sup>F. Okuyama and Y. Fujimoto, *J. Appl. Phys.* **56**, 566 (1984).
- <sup>28</sup>F. Okuyama, S. Aoyama, and Y. Fujimoto, *J. Cryst. Growth* **114**, 107 (1991).
- <sup>29</sup>A. D. Kent, T. M. Shaw, S. von Molnar, and D. D. Awschalom, *Science* **262**, 1249 (1993).
- <sup>30</sup>D. R. Bidinosti and N. S. McIntyre, *Can. J. Chem.* **45**, 641 (1967).
- <sup>31</sup>J. R. Gord, S. R. Horning, J. M. Wood, R. G. Cooks, and B. S. Freiser, *J. Am. Soc. Mass Spectrom.* **4**, 145 (1993).
- <sup>32</sup>N. Saitou, *Surf. Sci.* **66**, 346 (1977).
- <sup>33</sup>E. W. McDaniel, *Collision Phenomena in Ionized Gases* (Wiley, New York, 1964).
- <sup>34</sup>S. Y. Nagamachi, Y. Yamakage, M. Ueda, H. Maruno, and J. Ishikawa, *Rev. Sci. Instrum.* **67**, 2351 (1996).
- <sup>35</sup>H. Tokodoro, N. Saitou, and S. Yamamoto, *Jpn. J. Appl. Phys., Part 1* **21**, 1513 (1982).
- <sup>36</sup>R. R. Kunz and T. M. Mayer, *Appl. Phys. Lett.* **50**, 962 (1987).
- <sup>37</sup>Y. M. Lau, P. C. Chee, J. T. L. Thong, and V. Ng, *J. Vac. Sci. Technol. A* **20**, 1295 (2002).